

# **SIMULATION OF COMPLEX IMPACT PROBLEMS WITH IMPLICIT TIME ALGORITHMS. APPLICATION TO CRASHWORTHINESS PROBLEMS.**

## **SIMULATION DE PROBLEMS COMPLEXES AVEC DES ALGORITHMES TEMPORELS IMPLICITES. APPLICATION AUX PROBLEMES D'IMPACTS.**

Ludovic Noels, Laurent Stainier and Jean-Philippe Ponthot

*LTAS-Milieux Continus & Thermomécanique, Department of AeroSpace, Mechanics and Materials, University of Liège, Chemin des Chevreuils 1, B-4000 Liège, Belgium*

**Summary:** Recently, robust implicit energy and momentum conserving algorithms have been developed in the non-linear range. The authors extended these algorithms to hypoelasticity-based constitutive models and introduced numerical dissipation, opening the way to more complex simulations such as blade-loss in a turbofan.

**Résumé:** Récemment, des algorithmes implicites robustes, conservant l'énergie et le moment angulaire dans le domaine non-linéaire, ont été développés. Les auteurs ont étendu ces algorithmes aux modèles constitutifs à base hypo-élastique, et ont introduit de la dissipation numérique, ouvrant ainsi la voie à des simulations complexes comme la perte d'aube dans un turbofan.

### **INTRODUCTION**

When studying impact problems, time integration of the equations of evolution occurs in the non-linear range. Usually, explicit algorithms are used in such a context. Nevertheless, due to its lack of stability in the non-linear range, and its limitation in the time step size, an implicit scheme could advantageously be used. The most widely used implicit algorithm is the Newmark algorithm [1]. Nevertheless, when this algorithm is used in the non-linear range, the conservation of the energy is no longer satisfied. To avoid divergence due to the numerical instabilities, numerical damping was introduced, leading to the generalized- $\alpha$  methods [2]. But these schemes can exhibit instabilities in the non-linear range too [3]. Therefore a new family of integration algorithms for structural dynamics has appeared that satisfies the mechanical laws of conservation (i.e. conservation of linear momentum, angular momentum and total energy) and that remains stable in the non-linear range.

The first algorithm verifying these properties was described by Simo and Tarnow [4]. They called this algorithm Energy Momentum Conserving Algorithm or EMCA. It consists in a mid-point scheme with an adequate evaluation of the internal forces. This adequate evaluation was given for a Saint Venant-Kirchhoff hyperelastic material. A generalization to other hyperelastic models was given by Laursen [5], who iteratively solved a new equation for each Gauss point to determine the adequate second Piola-Kirchhoff stress tensor. Another solution that avoids this iterative procedure, and leads to a general formulation of the second Piola-Kirchhoff stress tensor, was given by Gonzalez [6]. This formulation is valid for general hyperelastic materials. The EMCA was recently extended to dynamic finite deformation plasticity by Meng and Laursen [7]. The finite element discretization leads to high frequency modes that are purely numeric. To avoid the convergence problems resulting from these modes, Armero and Romero [8,9] introduced numerical dissipation in these conserving algorithms. This dissipation only affects the total energy but preserves the angular momentum. Moreover, it is proved to be stable in the non-linear range, contrarily to the  $\alpha$ -generalized algorithms. It is called Energy Dissipative Momentum Conserving algorithm or EDMC. Besides, Armero and Petöcz [10,11] proposed a treatment of contact interactions in a consistent way in the non-linear range.

All the conserving methods described above were established for hyperelastic materials. We have recently [12,13] established a new expression of the internal forces for the hypoelastic materials using the final rotation scheme [14]. When associated with the mid-point scheme, this expression ensures the conservation laws of mechanics for a hypoelastic constitutive model. Moreover, we proved that this adaptation remains consistent with the Drucker postulate when plastic deformation occurs. Nevertheless, to be able to simulate complex impact problems, two improvements are necessary. The first one is to introduce numerical dissipation in a consistent way for such hypoelastic constitutive models [15]. This numerical dissipation avoids the numerical high frequency modes parasiting the physical solution. The second one is an enhancement of the contact formulation proposed by Armero and Petöcz to surfaces with discontinuous normal, as is the case when the two bodies in contact are deformable and are thus discretized by finite elements [16]. With such improvements, we are able to simulate complex problems of impact such as a blade-loss in a turbo engine.

### DESCRIPTION OF THE MODEL

The turbo-engine is modeled with a shaft that has an imposed revolution motion on one extremity. At its other extremity, there is a disk with 24 blades. The shaft, the disk and the blades are part of the rotor, which is in rotation in a stator. The stator is composed of a casing and a bearing. The rotor has a cyclic symmetry of 15 degrees. Fig. 1 illustrates a 15-degree part of the rotor. The blade is defined from a ruled surface that has two splines for extremities. The blade is made of an alloy (density 3600 kg/m<sup>3</sup>, Young's modulus 88000 N/mm<sup>2</sup>, Poisson's coefficient 0.31, initial yield stress 880 N/mm<sup>2</sup> and hardening parameter 26700 N/mm<sup>2</sup>). The disk and the shaft are composed of another alloy (density 6300 kg/m<sup>3</sup>, Young's modulus 165000 N/mm<sup>2</sup>, Poisson's coefficient 0.31, initial yield stress 800 N/mm<sup>2</sup> and hardening parameter 271 N/mm<sup>2</sup>). The blade is discretized with 99 elements: 11 in length (elements at the head of the blade are 50% smaller than at the root), 9 elements in height and 1 element on the thickness. The disk has 2 elements on the thickness and 72 elements on the circumference. The shaft has 1 element on its thickness and 11 elements on its length (8 for the constant section shaft and 3 for the conical part). The shaft has 72 elements on its circumference. The elements are 8-node bricks with constant pressure.

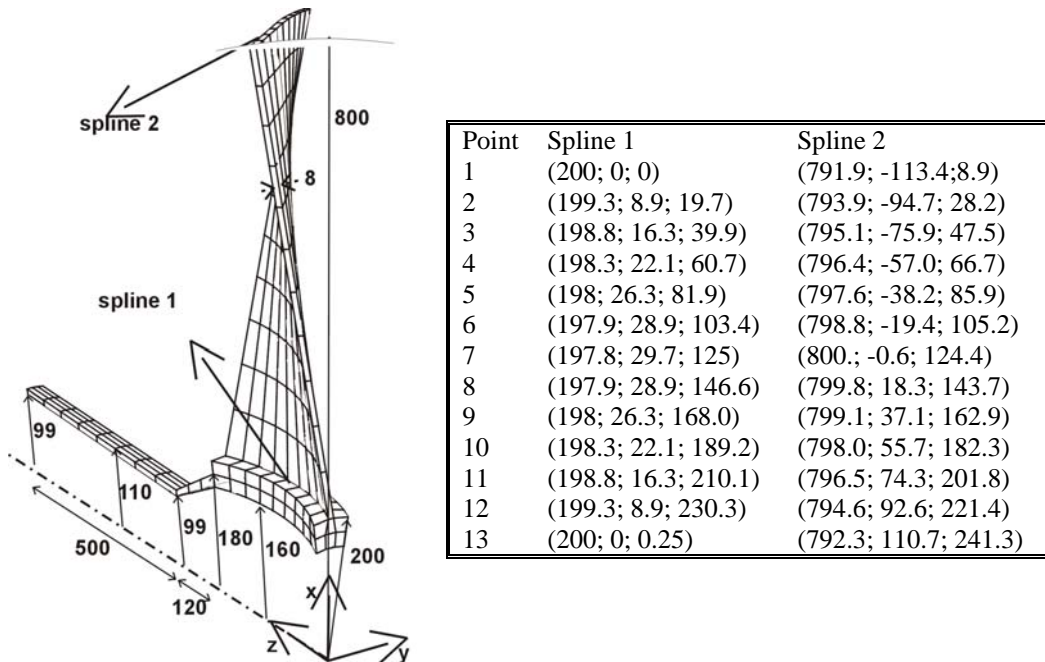


Fig. 1. Model (dimensions in mm).  
 Fig. 1. Modèle (dimensions en mm).

The casing is a cylinder made of an aluminium alloy (density 2710 kg/m<sup>3</sup>, Young's modulus 55200 N/mm<sup>2</sup>, Poisson's coefficient 0.31, yield stress 550 N/mm<sup>2</sup> and hardening parameter 281 N/mm<sup>2</sup>). Its geometry is illustrated at Fig. 2a. The bearing has a conical geometry (Fig. 2b) and is made of an alloy (density 3600 kg/m<sup>3</sup>, Young's modulus 88000 N/mm<sup>2</sup>, Poisson's coefficient 0.31, yield stress 550 N/mm<sup>2</sup> and hardening parameter 2600 N/mm<sup>2</sup>). The displacement of the shaft is restrained by the bearing thanks to a central node (Fig. 2b). There are springs between the central node and the extremity nodes of the bearing and there are springs between the central node and two rows on nodes of the shaft. Each spring has a stiffness of 10<sup>8</sup> N/mm. A mass of 0.05kg is associated with the central node. The bearing and the casing have 1 element on the thickness. The casing has 36 elements on its circumference and 8 elements on its length. The bearing has 3 elements on its length and 20 on its circumference. The elements are 8-node bricks with constant pressure.

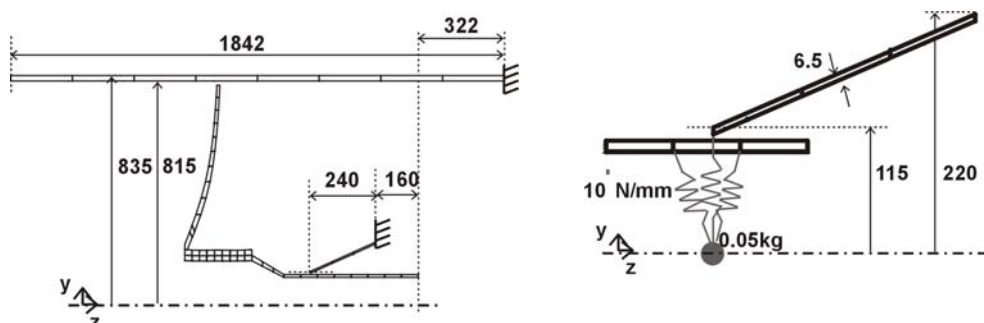


Fig. 2. Stator model, a- casing, b- bearing.  
 Fig. 2. Modèle du stator, a- carter, b- palier.

## INITIAL CONFIGURATION

At time  $t=0s$ , the initial configuration of the rotor is computed for a rotation velocity of 4775 rpm. This initial configuration is computed with a Newton-Raphson scheme where the external forces are the analytical inertial forces computed from the nodes position and from the imposed rotation velocity. The von Mises stresses resulting from this uniform rotation velocity are illustrated at Fig. 3. The blade pointed by an arrow is independent from the disk. To evaluate the initial configuration, it is linked to the disk thanks to an adhesion law (normal penalty  $10^9$ , tangential penalty  $10^8$ ). After the initial configuration is evaluated, this link is removed and the free blade interacts with the other blades and with the casing. The interaction between the blades and the casing is simulated with a Coulomb friction law (normal penalty  $10^9$ , tangential penalty  $10^7$  and friction coefficient 0.1). The interaction between the free blade and the other blades is simulated with the same law. Contact interactions between attached blades are simulated with a frictionless law (normal penalty  $10^9$ ).

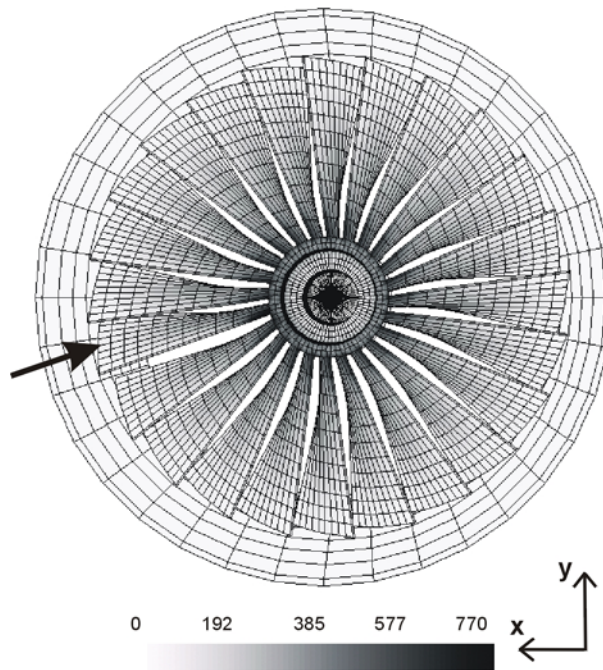


Fig. 3. Initial von Mises stresses (Mpa) of the rotor (front view).  
 Fig. 3. Contraintes de von Mises (Mpa) initiales du rotor (vue de face).

## NUMERICAL SIMULATION OF THE FIRST REVOLUTION

Now we analyze the first revolution of the rotor after the blade loss. We use the EDMC (first order accurate) algorithm with a spectral radius equal at the infinity frequency 0.8. The time step size is computed from an automatic criterion [17] and with an accuracy of  $10^{-4}$  on the integration error. The Hessian matrix is updated only when necessary [17]. Each time step is computed with a Newton-Raphson scheme (tolerance =  $10^{-5}$ ) enhanced by a line-search [18] (tolerance  $10^{-3}$ ).

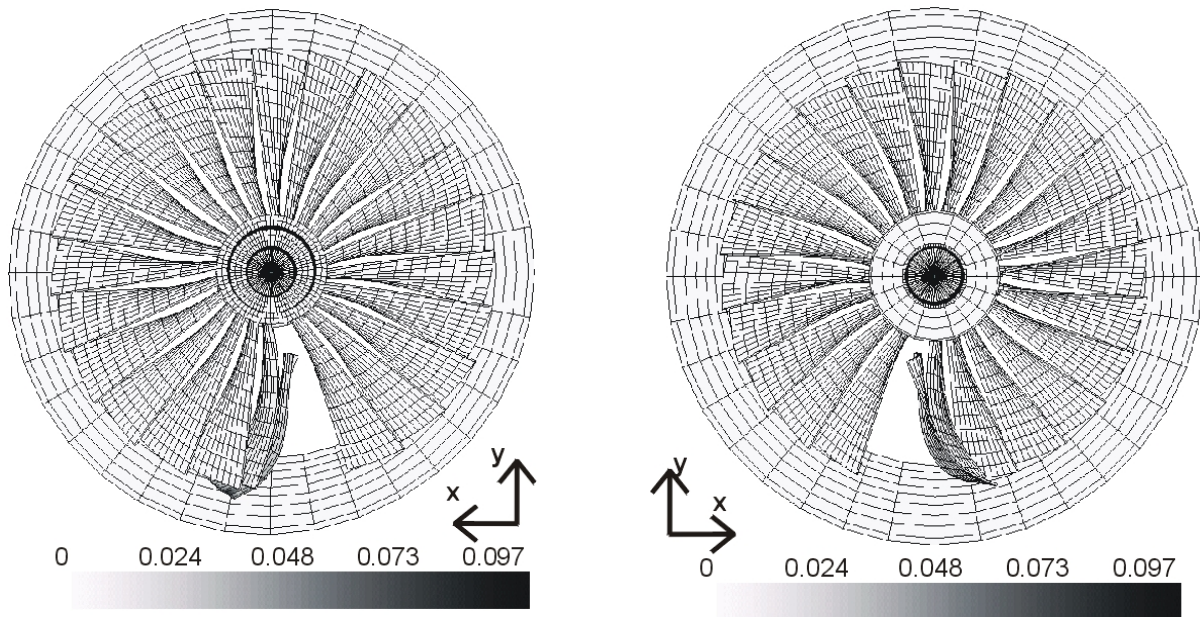


Fig. 4. Configuration and equivalent plastic strains after a quarter of revolution, a- front view, b- rear view.  
 Fig. 4. Configuration et déformations plastiques équivalentes après un quart de tour, a- vue de face, b- vue de dos.

Fig. 4a and Fig. 4b illustrate respectively the front and the rear view of the configuration after a quarter of revolution. The free blade interacts with the first next (attached) blade. Fig. 5a and Fig. 5b illustrate respectively the front view and the rear view of the configuration after half a revolution. The free blade remains between the linked blades and the casing. Due to the friction law, the attached blades bend. The head of the free blade enters into contact with the fifth linked blade. Fig. 6a and Fig. 6b illustrate respectively the front view and the rear view of the deformation after three quarters of a revolution. The head of the free blade has led the fifth blade to bend significantly, and the free blade is pushed towards the rear of the casing. Fig. 7a and Fig. 7b illustrate respectively the front view and the rear view of the results after a revolution. The free blade was pushed away from the disk so that the remaining interactions only occur between the linked blades and the casing.

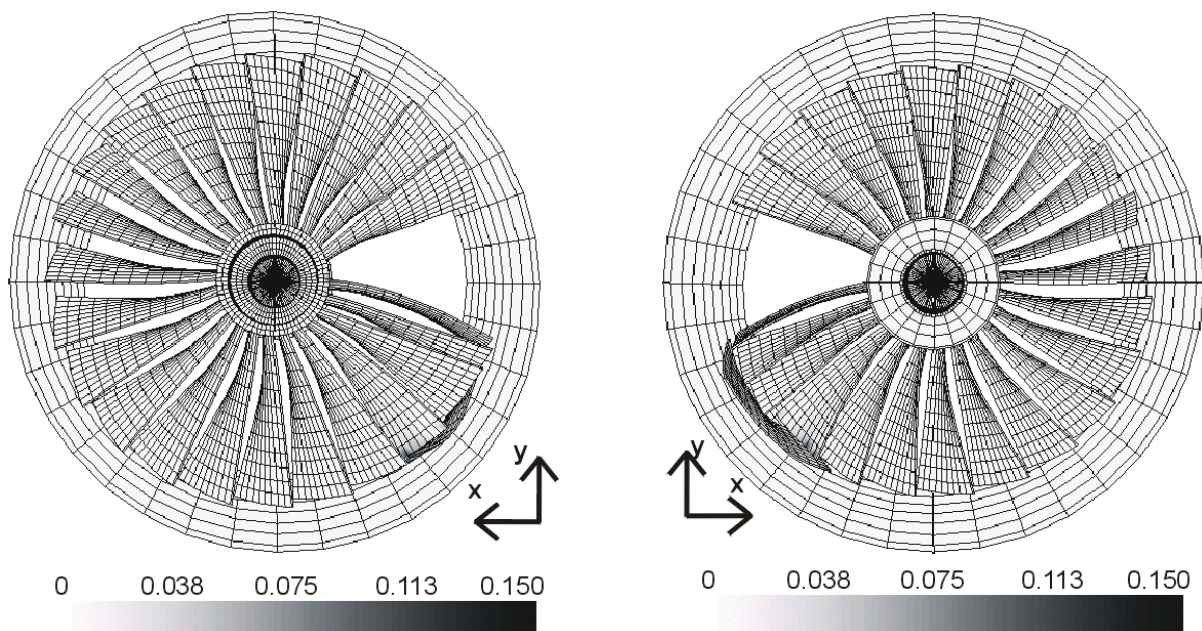


Fig. 5. Configuration and equivalent plastic strains after half a revolution, a- front view, b- rear view.  
 Fig. 5. Configuration et déformations plastiques équivalentes après un demi tour, a- vue de face, b- vue de dos.

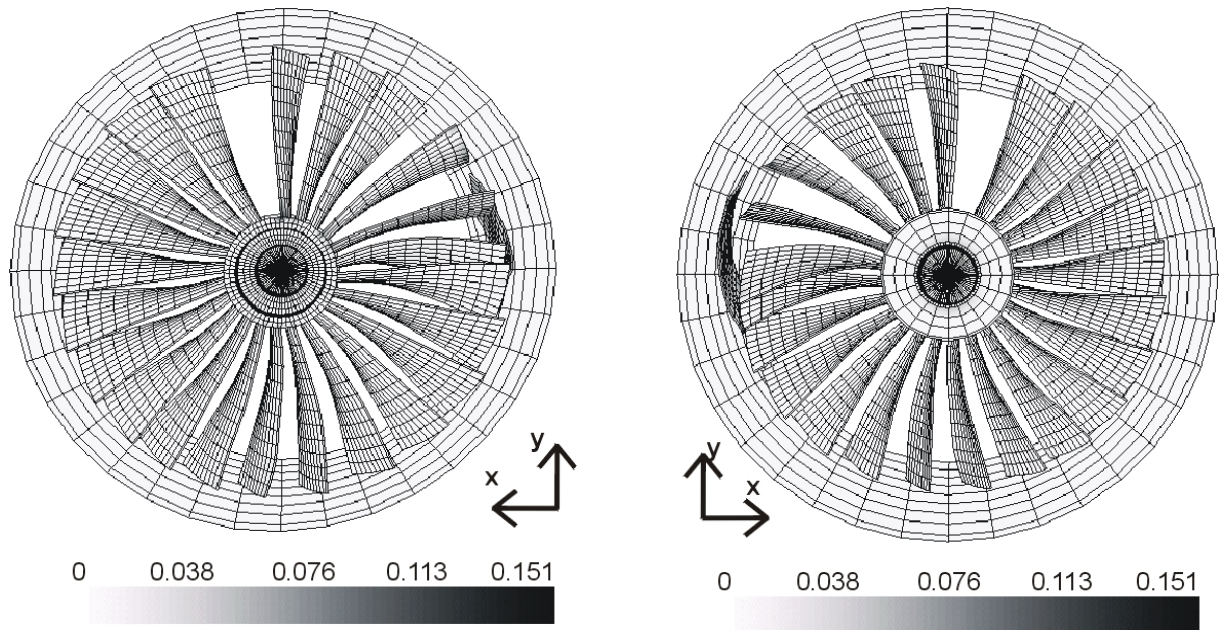


Fig. 6. Configuration and equivalent plastic strains after three quarters of revolution, a- front view, b- rear view.  
 Fig. 6. Configuration et déformations plastiques équivalentes après trois quarts de tour, a- vue de face, b- vue de dos.

The total force on the bearing is illustrated at Fig. 8a. It appears that this force is linear during the first instants, when the bearing reacts to the presence of an unbalanced shaft. But when the free blade interacts with both the linked blades and the casing, the force starts oscillating. The time evolution of the force on the casing (Fig. 8b) results from the interaction of the blades on the casing and the force oscillates during the whole simulation.

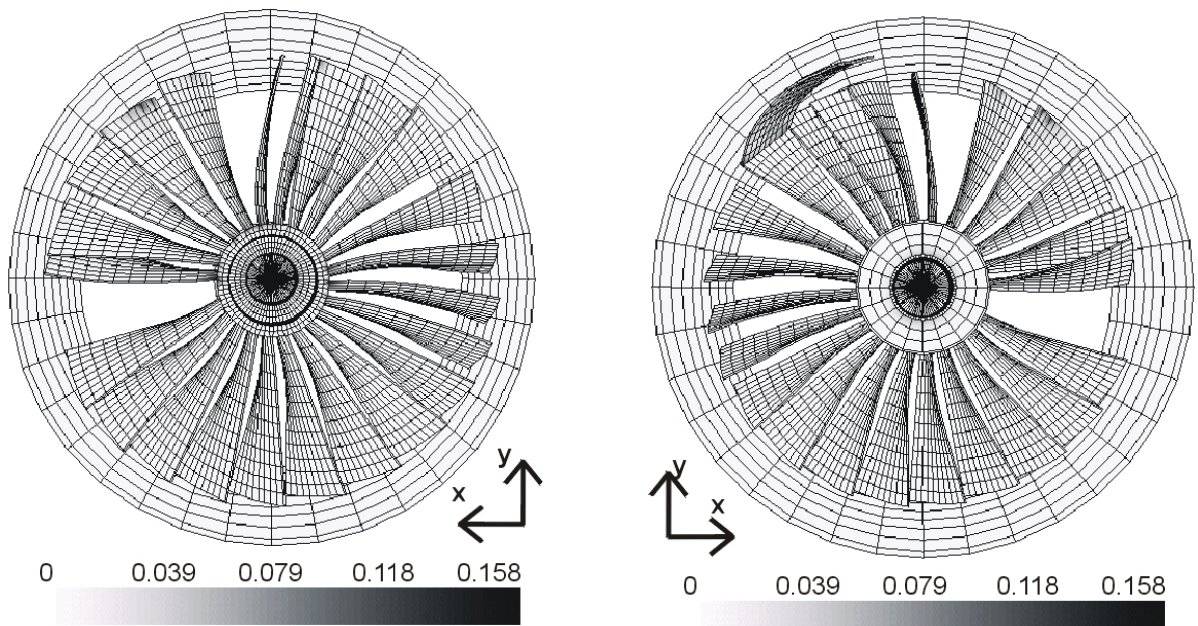


Fig. 7. Configuration and equivalent plastic strains after a full revolution, a- front view, b- rear view.  
 Fig. 7. Configuration et déformations plastiques équivalentes après un tour complet, a- vue de face, b- vue de dos.

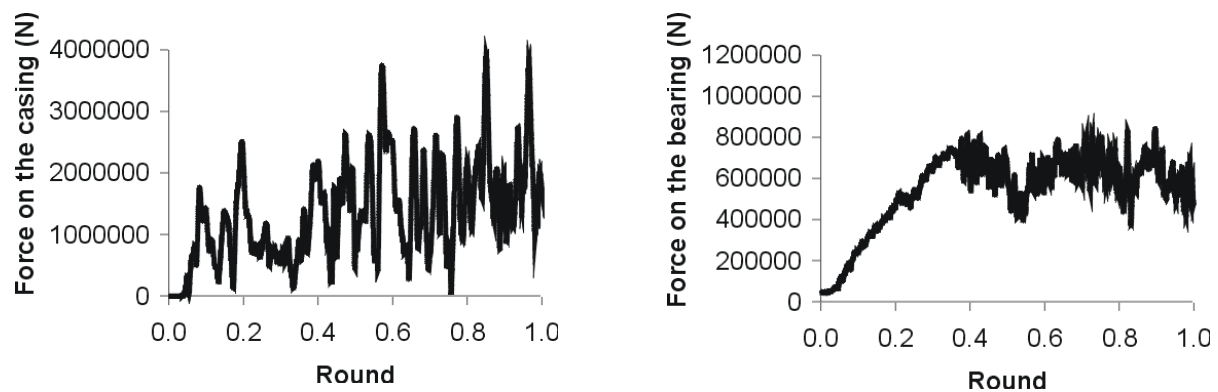


Fig. 8. Time evolution of the clamping forces, a- casing, b- bearing.  
 Fig. 8. Evolution temporelle des forces d'encastrement, a- carter, b- palier.

## CONCLUSIONS

In this paper we proved that new developments in the study of the implicit schemes stability allow us to compute complex dynamics such as a blade loss problem. Advantages of the implicit scheme compared to the explicit one are its stability in the non-linear range that is mathematically proved and its ability to use large time step size. For the present simulation, the mean implicit time step size is equal to about  $1.8 \mu\text{s}$  and the explicit critical time step is equal to  $0.07 \mu\text{s}$ . But thanks to the automatic Hessian matrix update and time step computation, the implicit steps are not much more expensive than the explicit ones. The implicit simulation is therefore twice cheaper than the explicit one.

## References

- [1] Newmark, N., A method of computation for structural dynamics, *Journal of the Engineering Mechanics Division ASCE*, **85** (1959), pp. 67-94
- [2] Chung, J., Hulbert, G., A time integration algorithm for structural dynamics with improved numerical dissipation: the generalized- $\alpha$  method, *Journal of Applied Mechanics*, **60** (1993), pp. 371-375
- [3] Erlicher, S., Bonaventura, L., Bursi, O., The analysis of the  $\alpha$ -generalized method for non-linear dynamic problems, *Computational Mechanics*, **28** (2002), pp. 83-104
- [4] Simo, J., Tarnow, N., The discrete energy-momentum method. Conserving algorithms for nonlinear elastodynamics, *ZAMP*, **43** (1992), pp. 757-792
- [5] Laursen, T., Meng, X., A new solution procedure for application of energy-conserving algorithms to general constitutive models in nonlinear elastodynamics, *Computer Methods in Applied Mechanics and Engineering*, **190** (2001), pp. 6309-6322
- [6] Gonzalez, O., Exact energy and momentum conserving algorithms for general models in nonlinear elasticity, *Computer Methods in Applied Mechanics and Engineering*, **190** (2000), pp. 1763-1783
- [7] Meng, X., Laursen, T., Energy consistent algorithms for dynamic finite deformation plasticity, *Computer Methods in Applied Mechanics and Engineering*, **191** (2001), pp. 1639-1675
- [8] Armero, F., Romero, I., On the formulation of high-frequency dissipative time-stepping algorithms for non-linear dynamics. Part I: low-order methods for two model problems and nonlinear elastodynamics, *Computer Methods in Applied Mechanics and Engineering*, **190** (2001), pp. 2603-2649
- [9] Armero, F., Romero, I., On the formulation of high-frequency dissipative time-stepping algorithms for non-linear dynamics. Part II: second order methods, *Computer Methods in Applied Mechanics and Engineering*, **190** (2001), pp. 6783-6824
- [10] Armero, F., Petőcz, E., Formulation and analysis of conserving algorithms for frictionless dynamic contact/impact problems, *Computer Methods in Applied Mechanics and Engineering*, **158** (1998), pp. 269-300
- [11] Armero, F., Petőcz, E., A new dissipative time-stepping algorithm for frictional contact problems: formulation and analysis. *Computer Methods in Applied Mechanics and Engineering*, **179** (1999), pp. 151-178
- [12] Noels, L., Stainier, L., Ponthot, J.-P., Energy-momentum conserving algorithm for non-linear hypoelastic constitutive models, *International Journal for Numerical Methods in Engineering*, **59** (2004), pp. 83-114
- [13] Noels, L., Stainier, L., Ponthot, J.-P., On the use of large time steps with an energy-momentum conserving algorithm for non-linear hypoelastic constitutive models, *International Journal of Solids and Structures*, **41** (2004), pp. 663-693
- [14] Ponthot, J.-P., Unified stress update algorithms for the numerical simulation of large deformation elasto-plastic and elasto-viscoplastic processes, *International Journal of Plasticity*, **18** (2002), pp. 91-126
- [15] Noels, L., Stainier, L., Ponthot, J.-P., On Simulation of complex impact problems with implicit time algorithm. Application to a blade-loss problem, *International Journal of Impact Engineering*, (Submitted in 2004)
- [16] Noels, L., Stainier, L., Ponthot, J.-P., Simulation of crashworthiness problems with improved contact algorithms for implicit time integration of non linear dynamics, *International Journal of Impact Engineering*, (Submitted in 2004)
- [17] Noels, L., Stainier, L., Ponthot, J.-P., Self-adapting time integration management in crash-worthiness and sheet metal forming computations, *International Journal of Vehicles Design*, **30** (2002), pp. 67-114
- [18] Crisfield, M., *Non-linear finite element analysis of solids and structures*, John Wiley and Sons (2001)